Postharvest Biology and Technology 190 (2022) 111939

Contents lists available at ScienceDirect

Postharvest Biology and Technology

journal homepage: www.elsevier.com/locate/postharvbio

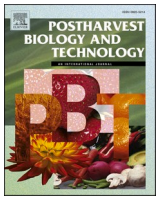

Prediction of the temperature sensitivity of strawberry drop damage using dynamic finite element method

Xue An [a], Huijie Liu [a], Tobi Fadiji [b], Zhiguo Li [a,*], Darko Dimitrovski [c]

[a] College of Mechanical and Electronic Engineering, Northwest A&F University, Yangling 712100, China
[b] Postharvest Research Laboratory, Department of Botany and Plant Biotechnology, University of Johannesburg, Johannesburg 2006, South Africa
[c] Department of Food and Biotechnology, Ss. Cyril and Methodius University in Skopje, Rudjer Boskovic 16, 1000 Skopje, Republic of Macedonia

ARTICLE INFO

Keywords:
Strawberry
Free drop
Temperature effect
Damage area and volume
Finite element analysis

ABSTRACT

In this study, the textural mechanics of strawberry tissues were analyzed using a uniaxial compression test at six temperature levels, and a dynamic finite element model of the strawberry drop system was developed to investigate the collision-damage sensitivity of the fruit. The strawberry geometric model included two parts of the receptacle: the cortex and the pith. The fruit finite element model with average tissue mechanical data was found to be capable of reproducing four key collision mechanical parameters (maximum impact force and contact area, drop damage area, percentage of damage volume) with an average relative error of 1.76%, 8.45%, 2.99% and 4.74%, respectively. Five covariance analysis models also showed that the drop direction was the most important factor affecting the occurrence of the fruit drop damage, followed by fruit temperature and drop height. Specifically, in a low temperature range (1 ~ 7 °C), the fruit collision damage degree did not change significantly with temperature change, but when the temperature was between 14 °C and 35 °C, the damage area and percentage of damage volume increased by 0.82 mm^2 and 0.06%, respectively, for every 1 °C increase in temperature. Furthermore, it was found that there is a strong linear correlation between internal and surface damage in the strawberry fruit, and the obtained mathematical models can be utilized to predict the internal damage degree of fruit based on the surface damage area. This study incorporated dynamic finite element technology with statistical analysis to provide a systematic approach for investigating the collision-damage sensitivity of fresh fruit in relation to fruit temperature.

1. Introduction

Fresh strawberry (*Fragaria* × *ananassa* Duch.) is one of the most well-liked fruit on the market, with a naturally delicious flavor and several health benefits (Lin et al., 2017). They are particularly high in vitamin C (Bovi et al., 2018), essential for human heart health. Strawberry worldwide production and gross production value in 2019 are 224 thousand tons and 16.5 billion dollars, respectively (FAOSTAT, 2020). Strawberry has a delicate texture, making it one of the most sensitive fruit to dynamic mechanical damage during harvesting, packaging, sorting, and transportation (Dintwa et al., 2008). Nevertheless, drop damage is not immediately visible (Xia et al., 2020). As a result of the destruction of the damaged tissue cell in the impacted area (Surdilovic et al., 2018; Yousefi et al., 2016), fruit enzymatic browning occurs when phenolic compounds react over time and generate brown pigments under the catalysis of enzymes (Jiang et al., 2016; López-Serrano and Ros Barceló, 2001). It will not only facilitate the invasion of fungi and other microorganisms, but it will also hasten the decomposition of the whole fruit and reduce its economic worth (Chockchaisawasdee et al., 2016; Du et al., 2019). Drop analysis is one of the most prevalent approaches to exploring fruit dynamic mechanical damage behavior (Stropek and Gołacki, 2013). During post-handling operations such as harvesting, packaging, sorting, and transportation from the greenhouse to markets, fruit is often exposed to a wide range of environmental temperatures (approximately 1 ~ 35 ℃) (Kelly et al., 2019). However, temperature significantly impacts fruit's physiological activities, nutritional components, and textural qualities following a fall injury (Deng et al., 2020; Guo et al., 2019; Matsumoto and Ikoma, 2012). At higher temperatures, the cell membrane of strawberry fruit becomes significantly more sensitive, causing the fruit's respiration rate to accelerate and the consumption rate of sugar and organic acid to increase (Chang and Lin, 2020). As a result, research into strawberry fruit drop damage under various environmental temperatures is crucial.

* Corresponding author.
E-mail address: lizhiguo0821@163.com (Z. Li).

https://doi.org/10.1016/j.postharvbio.2022.111939
Received 14 February 2022; Received in revised form 12 April 2022; Accepted 13 April 2022

Nomenclature

A	cross-sectional area of the sample, mm^2
A_c	maximum contact area between fruit and rigid surface, mm^2
A_d	surface damage area of fruit, mm^2
A_0	area of the reference scale, mm^2
C	constant
C_{ik}	independent variables qualitative variables
d_0	cross-sectional thickness of the sample, mm
d	initial drop direction, $d = 0$ means the fruit drop along its transverse equatorial section, and $d = 1$ means the fruit drop along its longitudinal equatorial section
E	compression elastic modulus, MPa
E_c	elastic modulus of cortex, MPa
E_h	plastic hardening modulus, MPa
E_p	elastic modulus of pith, MPa
E_{tc}	tangent modulus of cortex, MPa
E_{tp}	tangent modulus of pith, MPa
E_{maxc}	maximum elastic modulus of cortex, MPa
E_{avgc}	average elastic modulus of cortex, MPa
E_{minc}	minimum elastic modulus of cortex, MPa
E_{maxp}	maximum elastic modulus of pith, MPa
E_{avgp}	average elastic modulus of pith, MPa
E_{minp}	minimum elastic modulus of pith, MPa
$F_{c\ max}$	elastic peak force, N
F_{max}	maximum impact force of strawberry fruit model to rigid surface during collision, N
h	intimal drop height of fruit, mm
L	initial length of the sample, mm
L_{ec}	side length of the cortex tissue element, mm
L_{ep}	side length of the pith tissue element, mm
L_1	length of the sample after test, mm
m	fruit mass, g
m_0	number of factors
n	number of covariates
N_c	number of failure integration point in the cortex tissue elements
N_d	number of pixels in the damage area
N_p	number of failure integration point in the pith tissue elements
N_0	number of pixels of a reference scale
P_i	dependent variable
P_{dvc}	percentage of drop damage volume of cortex tissue in the fruit model, %
P_{dvf}	percentage of drop damage volume of whole fruit model, %
P_{dvp}	percentage of drop damage volume of pith tissue in the fruit model, %
R	fruit curvature radius, mm
T	Fruit temperature, ℃
S_{ij}^*	trial elastic deviatory stress state
v	initial velocity of fruit impact to the rigid surface, $m{\cdot}s^{-1}$
V_{dc}	drop damage volume of cortex tissue in the fruit model, mm^3
V_{df}	drop damage volume of whole fruit model, mm^3
V_{dp}	drop damage volume of pith tissue in the fruit model, mm^3
V_f	volume of whole fruit geometric model, mm^3
w	cross-sectional width of the sample, mm
x_{ij}	independent variables quantitative variables
σ_c	yield stress of the tissue, MPa
σ_y	initial yield stress, MPa
σ_{yc}	yield stress of cortex, MPa
σ_{yp}	yield stress of pith, MPa
σ_{maxyc}	maximum failure stress of cortex, MPa
σ_{avgyc}	average failure stress of cortex, MPa
σ_{minyc}	minimum failure stress of cortex, MPa
σ_{maxyp}	maximum yield stress of pith, MPa
σ_{avgyp}	average yield stress of pith, MPa
σ_{minyp}	minimum yield stress of pith, MPa
σ_0	strain rate dependent factor using the Cowper and Symonds model, %
ε_{eff}^p	effective plastic strain, %
ε	plastic strain, %
$\dot{\varepsilon}$	strain rate, %
ε_c	failure strain of tissue, %
ε_i	random error
ρ_p	density of pith, $g{\cdot}cm^{-3}$
ρ_c	density of cortex, $g{\cdot}cm^{-3}$
α_0	intercept
α_{1k} and α_{2j}	coefficients of the kth factor and jth covariate, respectively
λ_c	Poisson's ratio of cortex
λ_p	Poisson's ratio of pith

Previous studies on mechanical damage to strawberries focused on the experimental test. An et al. (2020) demonstrated that there was no visible browning (compression damage) on the strawberries' longitudinal equatorial section with a compressibility level of 2.5%, and that the browning volume of fruit gradually increased with deformation percentage increase when the compressibility level was less than 28.1% at 1 $mm{\cdot}s^{-1}$. Aliasgarian et al. (2015) illustrated that the maximum damage of 'Gaviota' strawberries was found during transportation at the bottom rows in the boxes. Similarly, the box's position inside the truck influenced the mechanical damage level, with strawberry fruit damage being more severe in boxes in higher positions. Chaiwong and Bishop (2015) discovered that vibration frequencies at 5 Hz for 150 s resulted in more 'Elsanta' strawberry bruises than vibration frequencies at 3 Hz. Ferreira et al. (2009) indicated that the bruise volumes of strawberries hydro-cooled from 30 °C to 20 °C were 0.43 cm^3 larger than those held at 1 °C (0.27 cm^3) when subjected to the same compression. The highest bruise volume of strawberry pulp during compression test was higher at 30 °C compared to that at 1 °C (Hussein et al., 2020). Kurpaska et al. (2020) revealed that the damage area of strawberry fruit surface after being impacted by suction cup at 0 h, 24 h, and 72 h were 26.40 mm^2, 28.43 mm^2, and 31.79 mm^2, respectively. Hikawa-Endo (2020) discovered that using polystyrene trays inside package boxes to hold strawberry fruit during long-distance transportation decreased strawberry fruit damage by 40%. Xanthopoulos et al. (2012) developed a strawberry packaging model to predict gas concentration using finite element (FE) method, which was then used to modify the atmosphere in strawberry packaging storage to improve shelf life.

In summary, the existing literature mainly focused on the experimental investigation of postharvest texture, compression, and vibration damage in fresh strawberries. However, few studies have been conducted on the sensitivity of collision damage and the correlation between internal and external damage of strawberry fruit under varied fruit temperatures. This gap impedes the quantitative assessment of the internal dynamic mechanical damage level of fresh strawberries at a specific handling stage involving different environmental temperatures, and it limits theoretical guidance for designing low-damage postharvest handling machines (*e.g.*, packaging machines) and their working environments (An et al., 2020). Strawberry can be regarded as a structural material with different types of tissue cells (Zulkifli et al., 2020). The occurrence and evolution of fruit damage under dynamic stress is a

complex non-linear structural problem. When a strawberry structure sustains significant deformation damage, its changing geometric configuration results in a geometric nonlinear response, and the strawberry material nonlinear stress-strain relationship is an example of material nonlinearity (Belytschko et al., 2000; Sadrnia et al., 2008). The dynamic FE method is an effective tool for solving the nonlinear stress-strain response of a structure body subjected to an external impact force at varying temperatures (Celik et al., 2011). Therefore, the objective of this study is to investigate the sensitivity of strawberry drop damage to temperature using the dynamic FE method, as well as the correlation between internal and external damage of a dropped strawberry fruit.

2. Methodology

2.1. Materials

'Benihoppe' strawberry fruit of similar size and shape were harvested manually at commercial maturity (75% red stage on the surface, without any defects) as proposed by USDA (2006) and Zhao et al. (2019) from a greenhouse at Yangling Agricultural Hi-tech Industries Demonstration Zone, China. After that, the fruit were transported into the laboratory immediately within 1 h. To reduce the textural changes during storage, strawberries with no surface damage were selected and then refrigerated at 4 °C.

2.2. Measurement of strawberry tissue thermo-mechanics

2.2.1. Experimental design

The thermo-mechanics of strawberry pith and cortex tissues were characterized in this section. According to the potential environmental temperature range in postharvest fruit handling and the optimum storage humidity proposed by Kelly et al. (2019), the textural mechanics of strawberry were determined at six temperature levels: 1 °C, 7 °C, 14 °C, 21 °C, 28 °C, and 35 °C, and the relative humidity was set to 90%. In this study, a climate chamber (HWS-80B, Tianjin Honuo Instrument Co., Ltd., China) was used to provide a constant temperature and humidity storage environment before mechanical loading (Fig. 1), and the mechanics testing process of a strawberry tissue under different storage temperatures was similar to that of Han et al. (2022). Firstly, the strawberry fruit were randomly divided into six groups corresponding to six set temperature levels, and each group of 10 fruit was used to measure the mechanical properties of the strawberry cortex and pith tissues at a temperature level. A total of 60 strawberry samples (6 temperature levels × 2 tissue types × 5 tissue samples) were tested for tissue mechanics measurement. The storage time of the strawberry fruit in the climate chamber determines whether the temperature of the internal fruit tissue can be reached according to the preset temperature of the climate chamber. A preliminary test involved measuring the time it took the strawberry fruit to reach the temperature specified using a thermocouple (WRNK-191, Guankuan Co., Ltd., China) before the tissue mechanics test (Duarte-Molina et al., 2016). It was found that the time it took for the internal strawberry fruit tissue to reach the set temperature was less than 20 min after strawberry storage in a constant temperature and humidity environment. Therefore, strawberry fruit tissue samples were placed in the climate chamber for 30 min prior to the strawberry fruit tissue mechanics measurement test in Section 2.2.2.

2.2.2. Experimental process

Taking the mechanical measurement of strawberry cortex tissue at a fruit temperature of 1 °C as an example. 1st step: several strawberry fruit were taken out from the refrigerator, and 5 standard cuboid cortex samples (length × width × height: 9 mm × 9 mm × 13 mm) were prepared based on the National Standard of GB/T 7314–2017 using a self-developed double-blade cutter (blade: IP54, Master proof, Germany) (Fig. 1). 2nd step: to minimize the interference of external environmental conditions in this experiment, the samples were immediately placed into the climate chamber at 1 °C and 90% RH for storage, 30 min after 5 samples were prepared. 3rd step: one tissue sample was taken from the climate chamber at a time and immediately placed on the center of the base plate of a texture analyzer (Universal-TA, Tengba instrument technology Co., Ltd., China) (Fig. 1). The P100 probe was used to compress the sample along its height direction with a loading speed of 1 mm·s^{-1} and a 50% compressibility level. The force-deformation data was recorded by a computer in real-time (Fig. 1). The climate chamber was placed very close to the texture analyzer to reduce the effect of secondary temperature change on the tissue sample. The time interval between the tissue sample being removed from the climate chamber and the texture analyzer finishing a compression test was reduced to less than one minute. The mechanical parameters of the 5 tissue samples were measured sequentially. 4th step: the test procedure was repeated from 1st step to 3rd step for measuring the mechanical properties of the pith tissue at 1 °C. Subsequently, the 1st to 4th steps of the test procedure were repeated sequentially to determine the mechanics of the strawberry cortex and pith tissue samples at the fruit temperatures of 7 °C, 14 °C, 21 °C, 28 °C, and 35 °C, respectively. Finally, the strawberry cortex and pith thermo-mechanics such as elastic modulus E_c, yield stress σ_c, and failure strain ε_c were derived using Eqs. (1)–(3) based on the National Standard of GB/T 7314–2017.

$$\sigma_c = \frac{F_{cmax}}{A} = \frac{F_{cmax}}{w d_0} \quad (1)$$

$$\varepsilon_c = \frac{L - L_1}{L} \times 100 \quad \% \quad (2)$$

$$E = \frac{\sigma_c}{\varepsilon_c} \quad (3)$$

2.3. Finite element modeling and simulation

2.3.1. 3D Finite element modeling

2.3.1.1. Geometric modeling and the definition of material properties. Firstly, the achene in a strawberry fruit was ignored, and the fruit was simplified into a structure composed only of pith tissue and cortex tissue

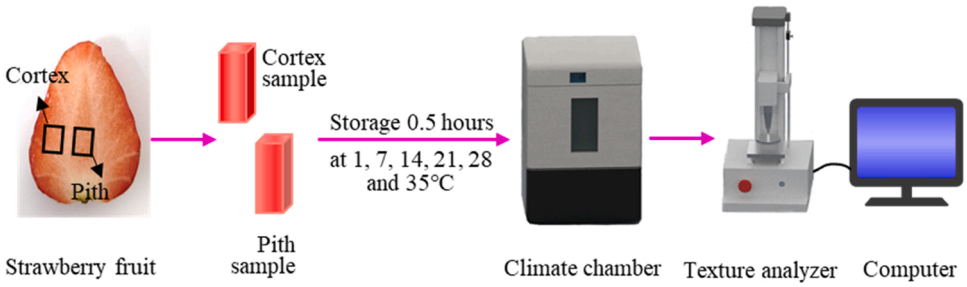

Fig. 1. The mechanics testing process of fruit tissue under different storage temperatures.

based on its anatomical characteristics (Fig. 2). Then, the boundary between the pith and cortex tissues was determined (Fig. 3a), after which a geometric model of the fruit was created (diameter in transverse equatorial section × height: 32 × 45 mm) using the operations such as extracting tissue contour points' coordinates, creating spline curves, and rotating in the Abaqus software (6.20/CAE, Dassault Systemes Simulia Corp., USA). Secondly, a 3D geometric model of the strawberry fruit free drop system (Fig. 3b) was created, consisting of a strawberry fruit model and a rigid surface. The rigid surface was 400 mm in length and 400 mm in breadth, and its thickness was not necessary to be specified because the rigid surface was set as the discrete rigid in Abaqus.

2.3.1.2. Definition of interaction. Firstly, the elastic modulus of strawberry pith tissue was greater than that of cortex tissue, so the outer surface of the pith geometric model was defined as the master surface, and the inner surface of the cortex geometric model was defined as the slave surface. A "Tie" constraint was used to connect two independent and defined master surface and slave surface together so that the motion (translational and rotational motion as well as all other motion freedom), temperature, stress value, and other parameters of each node on the slave surface were the same as those on the master surface. Surface-to-surface discretization technique for generating tie coefficients was selected to optimize stress accuracy for the specified surface pairing. The surface-to-surface discretization algorithm could establish the contact conditions for the whole slave surface. The shape changes of the master surface and the slave surface were examined concurrently in the analytical procedure to avoid severe penetration of some nodes on the master-slave surface. Following that, any nodes on the slave surface that were less than 0.2 mm from the master surface were bound to the master surface and will be moved to the master surface under initial conditions. The freedom of rotation on the master-slave surface was restricted because there was no relative motion between the cortex and the pith.

Next, the explicit general contact algorithm was used to define the interaction between the outer surface of the cortex geometric model and the top surface of the rigid surface during fruit free drop. A contact pair was simply defined in the general contact (Explicit) algorithm. The general contact algorithm automatically assigns master and slave surfaces and selects the finite sliding algorithm and the surface-to-surface discretization method, with few restrictions on the type of contact surface. The finite-sliding formulation is to continuously determine the contact state between the master surface and each node of the slave surface, and it is the most general because it allows for any arbitrary motion of the surfaces. The surface-to-surface discretization approach ensures that the constraints are applied uniformly throughout the contact area. The normal contact behavior between two contact surfaces follows the hard contact property to restrict the penetration behavior. The tangential contact behavior, which is described by the Coulomb friction model, states that the friction between the rigid surface and the outer surface of strawberry cortex tissue is isotropic. The friction coefficient was set to 0.4 (Li et al., 2021). The tangential friction behavior is governed by the "penalty" algorithm, which allows for some relative slippage when the fruit and rigid surface are attached. The maximum relative slip was set as 0.5% of the characteristic surface size. The shear stress between two contact surfaces was not limited before the master-slave contact surface started sliding, and the elastic sliding stiffness was defined as infinite to stop the shear softening. The "penalty" method is the stiffness approximation of hard contact, which is similar to the excessive closure behavior of hard pressure. By using this method, the total number of iterations necessary for analysis can be reduced.

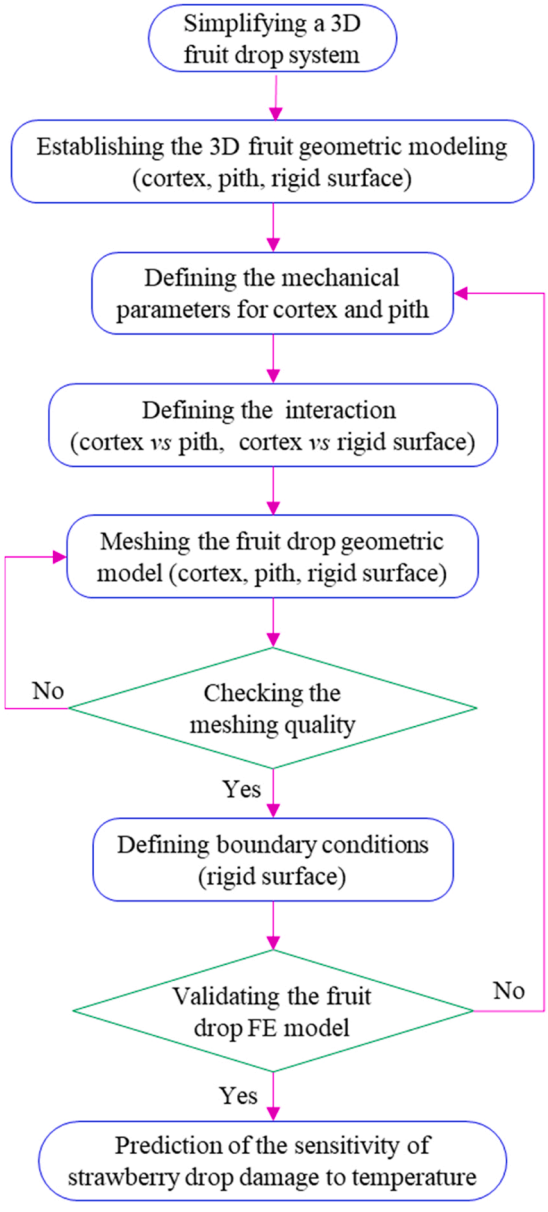

Fig. 2. Flow chart on the fruit drop finite element modeling.

2.3.1.3. Defining the boundary conditions and meshing. Firstly, a reference point was used to replace the discrete rigid surface for constraining all its freedoms. Secondly, considering that (i) the dynamic collision process of strawberry fruit dropping onto the ground will be completed in a very short time and followed by substantial energy changes. Thus the discrete rigid surface should be meshed as tiny as possible; (ii) a high-quality mesh in the fruit FE model can be obtained using the structured mesh generation technology based on the tetrahedral element type because the shape of the cortex and pith tissues in a strawberry fruit is irregular; (iii) there exist large fruit tissue deformation and some contact phenomena in the process of fruit free drop, so the robustness of the tissue element is required in the simulation to minimize the shear and volumetric locking property. Therefore, the discrete rigid surface was meshed using the 4-node 3D bilinear quadrilateral rigid (R3D4) element with a global size of 1 mm, and totally 160,000 elements were generated. The cortex and pith tissues were meshed using the 10-node modified tetrahedron (C3D10M) element with a global size of 1 mm, and 68,980 and 11,478 elements were generated, respectively. Finally, the 3D finite element model of the strawberry free drop system is obtained, as shown in Fig. 3c.

2.3.2. Validation of the finite element model

To validate the accuracy of the established 3D free drop system FE

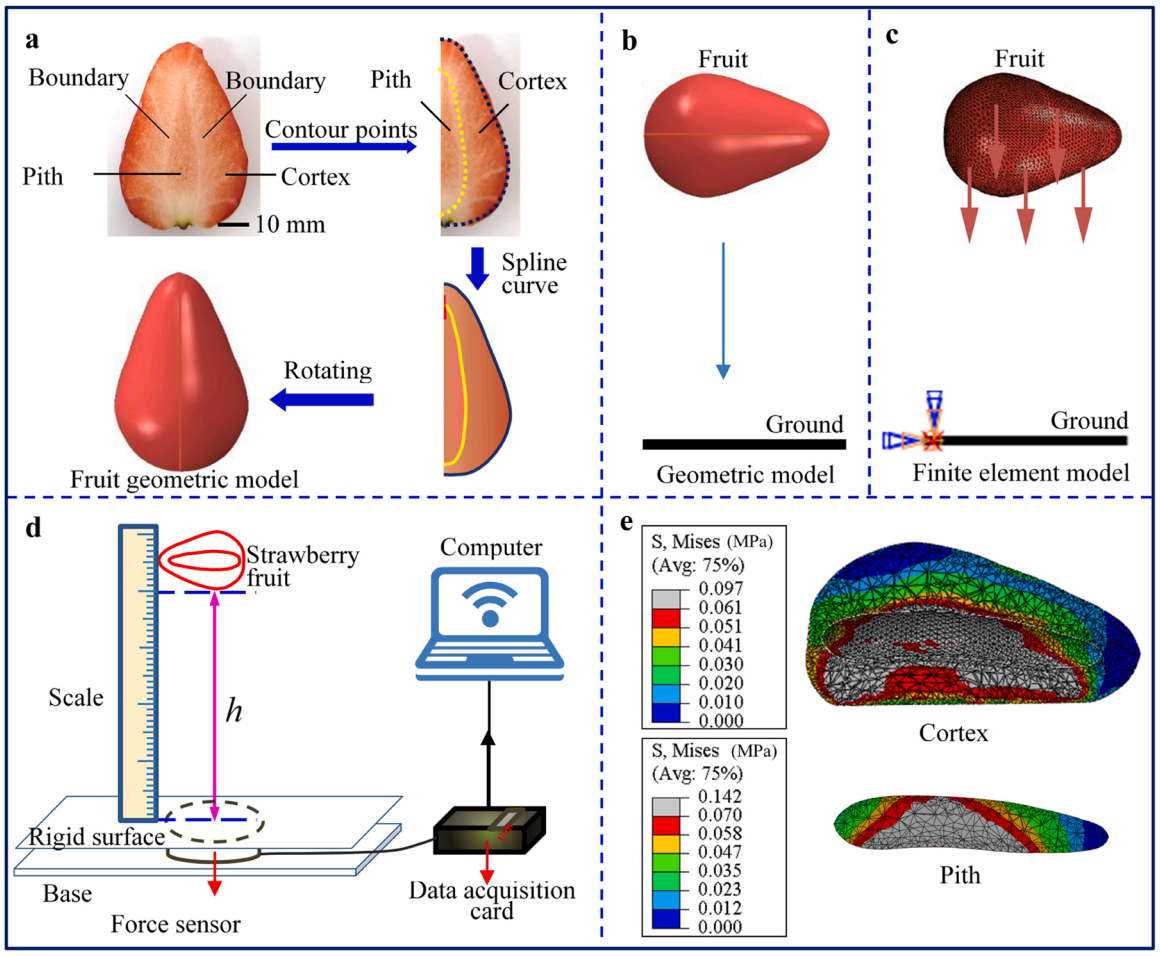

Fig. 3. Finite element modeling, free drop experiment, and simulation of strawberry fruit. (a) fruit geometric modeling, (b) geometric modeling of fruit free drop system, (c) finite element modeling of fruit free drop system, (d) fruit free drop test device, (e) stress contour of the cortex and pith tissue in the fruit equatorial section after simulation.

model, the simulation and experimental results of the strawberry fruit free drop test at room temperature (21 ℃) were compared, such as the maximum impact force of the strawberry fruit model dropping onto a rigid surface (Dintwa et al., 2008), the maximum contact area between fruit and rigid surface (Yousefi et al., 2016), damage area on fruit surface (Stropek and Gołacki, 2013), and percentage of fruit damage volume (Du et al., 2019).

2.3.2.1. Method of free drop experiment. firstly, a fruit free-drop test device was self-designed, as shown in Fig. 3d. Five strawberries of similar shape and mass were chosen, and they were suspended along the transverse equatorial section in turn and then free dropped onto the rigid surface from a height of $h = 441$ mm (corresponding to the 3 m·s^{-1} initial velocity of fruit collision on the rigid surface, calculated using $v^2 = 2gh$). The rigid surface was fixed on the top surface of a force sensor (JHBM-H1, Bengbu Sensor System Engineering Co., Ltd., China) with a measuring accuracy of 0.05 kg. The force-time data was captured in real-time by the force sensor during the collision of each strawberry fruit dropping onto the rigid surface and was transferred to the computer through the data acquisition card with a 12-bit A/D 8 channels analog input and a sample rate of 20 kHz (USB3100N, Beijing Art Technology Development Co., Ltd., China) to further extract the maximum impact force. The maximum contact area of fruit dropping onto the rigid surface was measured based on a blue inkpad imprint method proposed by Dzidek et al. (2017). Secondly, the dropped strawberries were placed at room temperature (21 ℃, RH 90%) for 4 h, after which the fruit browning area was observed, according to An et al. (2020). Then the fruit damage area and volume were extracted using the post-processing method described in Section 2.3.4. Because the free drop test was destructive and the fruit could not be used again after each drop, five strawberries of similar shape and mass were chosen for the drop test, implying that the test was repeated five times.

2.3.2.2. Method of free drop simulation. The mechanical parameters of the strawberry fruit pith and cortex tissue models were orderly set as the maximum, average, and minimum values at room temperature (21 ℃) (shown in No.21 in Table 1), and the drop height h of strawberry fruit was 441 mm. Subsequently, the free drop experiment of the strawberry fruit was simulated using the 3D free drop FE model, and the simulation results were used to extract four impact parameters (*e.g.*, maximum impact force of fruit model dropping onto the rigid surface, maximum contact area between fruit model and rigid surface, fruit damage area, percentage of damage volume for the whole fruit). Finally, the prediction accuracy of the 3D fruit FE model was assessed by comparing the extracted common parameters from the simulation and experimental results. Furthermore, to observe the two drop-rebound simulation processes of the strawberry fruit model free dropping from a height of 411 mm ($v = 3$ m·s^{-1}) to a rigid surface, the analysis steps and time were set to 6000 and 900 ms, respectively.

2.3.3. Loading and simulation

To investigate the effect of fruit temperature on the dynamic damage sensitivity of strawberry fruit, firstly, the temperature was set to six levels, namely, 1 °C, 7 °C, 14 °C, 21 °C, 28 °C, and 35 °C, and the

Table 1
Mechanical parameters of the 3D FE model used in sensitivity analysis of strawberry drop damage.

No. of simulation	T	Direction	Height (mm)	Mechanical parameters	
				Measured parameters	Cited parameters
1	1	along the	49	$E_c = 0.614$	$\rho_c = 1.01$, ρ_p
2		transverse	196	$\pm$ 0.062,	$= 1.01$,
3		equatorial	441	$E_p = 0.695$	$\lambda_c = 0.40$, λ_p
		section		$\pm$ 0.069,	$= 0.40$,
4		along the	49	$\sigma_{yc} = 0.100$	$E_{tc} = E_{tp}$
5		longitudinal	196	$\pm$ 0.012,	$= 0.30$;
6		equatorial	441	$\sigma_{yp} = 0.109$	
		section		$\pm$ 0.015;	
7	7	along the	49	$E_c = 0.490$	$\rho_c = 1.01$, ρ_p
8		transverse	196	$\pm$ 0.052,	$= 1.01$,
9		equatorial	441	$E_p = 0.586$	$\lambda_c = 0.40$, λ_p
		section		$\pm$ 0.061,	$= 0.40$,
10		along the	49	$\sigma_{yc} = 0.080$	$E_{tc} = E_{tp}$
11		longitudinal	196	$\pm$ 0.014,	$= 0.30$;
12		equatorial	441	$\sigma_{yp} = 0.091$	
		section		$\pm$ 0.004;	
13	14	along the	49	$E_c = 0.409$	$\rho_c = 1.01$, ρ_p
14		transverse	196	$\pm$ 0.025,	$= 1.01$,
15		equatorial	441	$E_p = 0.490$	$\lambda_c = 0.40$, λ_p
		section		$\pm$ 0.029,	$= 0.40$,
16		along the	49	$\sigma_{yc} = 0.067$	$E_{tc} = E_{tp}$
17		longitudinal	196	$\pm$ 0.011,	$= 0.30$;
18		equatorial	441	$\sigma_{yp} = 0.077$	
		section		$\pm$ 0.013;	
19	21	along the	49	$E_c = 0.373$	$\rho_c = 1.01$, ρ_p
20		transverse	196	$\pm$ 0.032,	$= 1.01$,
21		equatorial	441	$E_p = 0.448$	$\lambda_c = 0.40$, λ_p
		section		$\pm$ 0.037,	$= 0.40$,
22		along the	49	$\sigma_{yc} = 0.061$	$E_{tc} = E_{tp}$
23		longitudinal	196	$\pm$ 0.005,	$= 0.30$;
24		equatorial	441	$\sigma_{yp} = 0.070$	
		section		$\pm$ 0.006;	
25	28	along the	49	$E_c = 0.308$	$\rho_c = 1.01$, ρ_p
26		transverse	196	$\pm$ 0.036,	$= 1.01$,
27		equatorial	441	$E_p = 0.379$	$\lambda_c = 0.40$, λ_p
		section		$\pm$ 0.043,	$= 0.40$,
28		along the	49	$\sigma_{yc} = 0.053$	$E_{tc} = E_{tp}$
29		longitudinal	196	$\pm$ 0.013,	$= 0.30$;
30		equatorial	441	$\sigma_{yp} = 0.065$	
		section		$\pm$ 0.015;	
31	35	along the	49	$E_c = 0.274$	$\rho_c = 1.01$, ρ_p
32		transverse	196	$\pm$ 0.032	$= 1.01$,
33		equatorial	441	$E_p = 0.333$	$\lambda_c = 0.40$, λ_p
		section		$\pm$ 0.037	$= 0.40$,
34		along the	49	$\sigma_{yc} = 0.038$	$E_{tc} = E_{tp}$
35		longitudinal	196	$\pm$ 0.013	$= 0.30$.
36		equatorial	441	$\sigma_{yp} = 0.047$	
		section		$\pm$ 0.016;	

mechanical parameters of the cortex and pith tissues at different temperatures (Table 1) were inputted to the developed FE model for drop simulation instead of the effect of temperature fluctuation. Secondly, various drop height levels were set in the simulation to investigate the effect of drop height on the dynamic damage sensitivity of the strawberry fruit. The simulation approach needs a large number of incremental calculations in the fruit free drop from a given height to the rigid surface as well as the collision on the surface. To reduce the amount of calculation and shorten the calculation time in the simulation process, the strawberry model was moved to a position close to but not in contact with the rigid surface, and the initial speed relating to the fruit just in contact with the rigid surface was specified rather than the drop height. Therefore, the initial collision velocity between the fruit and rigid surface was set to three levels: 1 $m{\cdot}s^{-1}$, 2 $m{\cdot}s^{-1,}$ and 3 $m{\cdot}s^{-1}$, corresponding to three drop heights in the fruit simulation test, that is, 49 mm, 196 mm, and 441 mm, respectively. According to the findings of An et al. (2020), there are significant differences in mechanical damage of strawberry fruit when compressed from different directions. Therefore, to explore the effect of drop direction on the dynamic collision damage of strawberry fruit, the drop direction was set at two levels: along the transverse equatorial section and the longitudinal equatorial section. In addition, since the Poisson's ratio of fruit is approximately 0.30 ~ 0.49 (Mahiuddin et al., 2020), the Poisson's ratio of the strawberry fruit cortex and pith tissues was set to 0.40. Due to the large deformation of strawberry fruit in the collision process, the nonlinear geometric effect was considered in the collision analysis step. The initial impact moment, deformation progression, and rebound period were all taken into account in the simulation solving time, so each free drop simulation duration was set to 0.01 s with 100 sub-steps. In the collision analysis step, the global estimation algorithm was used to automatically estimate the improved stability time increment of the 3D tissue element, and the number of incremental steps was not restricted. Based on the verified fruit FE model in Section 2.3.2, 36 free drop FE simulations of the strawberry fruit were performed using the ABAQUS/Explicit dynamic solution method. All simulations were conducted on a HP Z840 High-Performance Computer Platform equipped with two E2683V4 16-core 2.1 GHz Intel(R) CPUs and a 160 G DDR4 2133 RegRAM.

To simplify the FE simulation, there were five assumptions as follows: (a) the possible influence of achene on the damage area and volume of real strawberry tissue can be ignored; (b) the yield stress of fruit tissue is independent of the size and shape of the measured tissue sample; (c) both the cortex and pith tissues were regarded as isotropic and homogeneous elastoplastic materials. In the simulation, the isotropic hardening material model was used as the constitutive model of elastic-plastic material of fruit tissue, which follows the isotropic hardening criterion. The isotropic hardening plastic material model is suitable for dynamic simulation analysis of high strain rate. When the tissue material reaches the yield stress, its stress and strain can continue to increase. At this time, the stress is a function of plastic strain. If the tissue is loaded again after unloading, the yield stress of the tissue material will increase. In isotropic hardening, the center of the yield surface is fixed, but the radius is a function of plastic strain, and the yield function is shown in Eqs. (4) and (5) (Du et al., 2019). (d) The biological yield point of a tissue sample can be regarded as the initial point of tissue plastic failure. Elastoplastic materials exhibit elastic properties at the beginning of loading, but the stress-strain curve becomes nonlinear when the stress reaches the yield point, and the permanent plastic deformation remains after unloading. Therefore, the bio-yield point of the strawberry tissue was regarded as its initial damage point, and the yield stress of the strawberry tissue was used to determine whether the tissue material will damage in free drop simulation (Celik, 2017). (e) The prediction of strawberry tissue failure behavior follows the fourth strength theory, namely the von Mises stress failure criterion, which is always used to analyze agricultural products' failure behavior (Sadrnia et al., 2008).

$$\varnothing = \frac{3}{2}\left(S_{ij}^{*} - \alpha_{ij}\right)^{2} - \sigma_0^2 = \wedge^2 - \sigma_0^2 \begin{cases} \leq 0 \text{for elastic or neutral loading} \\ > 0 \text{for plastic hardening} \end{cases} \tag{4}$$

$$\sigma_0 = \left[1 + \left(\frac{\varepsilon}{C}\right)^{\frac{1}{p}}\right]\left(\sigma_y + E_h \varepsilon_{eff}^{p}\right) \tag{5}$$

2.3.4. Post-processing analysis

2.3.4.1. Drop damage volume calculation. A self-developed ABAQUS post-processing plugin, "Damage Analysis," was used to extract the damage volume and percentage of damage volume of the tissues in the strawberry fruit model based on the result of each fruit drop FE simulation. Since both the pith and cortex tissue models are composed of the C3D10M element with 4 integration points, and it is assumed that all the meshed elements in the fruit model are regular tetrahedral elements, so when the stress value of a certain integration point in an element

exceeds the yield stress of the associated tissue, the integration point is considered as the failure integration point, and the element's damage volume is recorded as 1/4 of the entire element volume. After each drop simulation, the number of all failure integration points of the C3D10M elements in the pith and cortex tissue models was extracted from the simulation result by the "Damage Analysis" post-processing plugin. The damage volume of each tissue is the sum of the damage volumes of all elements in the tissue model. Because the C3D10M element is almost incompressible before and after simulation, the damage volume of strawberry fruit and its tissues can be deduced using Eqs. (6)–(8). After the drop simulation, the total damage volume of the strawberry fruit is the sum of the damage volumes of the cortex and pith tissue FE models. The volume V of the strawberry fruit geometric model was extracted by the CAD Software SolidWorks (Dassault systems SIMULIA Corp., USA). After each drop simulation, the percentage of damage volume of strawberry fruit and its tissues can be deduced using Eqs. (9)–(11).

$$V_{\mathrm{dc}} = \frac{1}{4} \times N_c \times \frac{\sqrt{2}}{12} L_{\mathrm{ec}}^{3} \tag{6}$$

$$V_{\mathrm{dp}} = \frac{1}{4} \times N_p \times \frac{\sqrt{2}}{12} L_{\mathrm{ep}}^{3} \tag{7}$$

$$V_{\mathrm{df}} = V_{\mathrm{dc}} + V_{\mathrm{dp}} \tag{8}$$

$$P_{\mathrm{dvc}} = \frac{V_{\mathrm{dc}}}{V_{\mathrm{f}}} \times 100 \quad \% \tag{9}$$

$$P_{\mathrm{dvp}} = \frac{V_{\mathrm{dp}}}{V_{\mathrm{f}}} \times 100 \quad \% \tag{10}$$

$$P_{\mathrm{dvf}} = \frac{V_{\mathrm{df}}}{V_{\mathrm{f}}} \times 100 \quad \% \tag{11}$$

2.3.4.2. Fruit damage area calculation. Because it is difficult to assess the internal damage degree of a dropped strawberry fruit using existing nondestructive detection technology, obtaining the relationship between the damage area on a fruit surface and the damage volume inside the fruit is a potential method for predicting the internal damage degree of fruit based on its corresponding surface damage. Therefore, in this study, the damage area on the surface of the fruit model was extracted from each free drop finite element simulation. In a fruit drop simulation, the fruit experiences local deformation due to local stress during collision with the rigid surface; the fruit contact surface between the fruit and the rigid surface is an irregular plane, and its contact area changes with impact contact time. Given the possibility of local damage on the fruit contact surface, the von Mises stress contour plot showing the greatest deformation of the fruit during free drop collision was chosen, and a 1/4 vol (the area around the corresponding integration point) of the element was set as the gray damage area where the von Mises stress value of an integration point in a cortex element is greater than the yield stress of the strawberry cortex tissue. Finally, the surface damage area A_{d} of the strawberry was extracted from the contact surface (collision between fruit and rigid surface) in the fruit cortex tissue model using an image processing method in Eq. (12) (Yousefi et al., 2016) by the Digimizer software (version 4.3.4, MedCalc Software, USA).

$$A_{\mathrm{d}} = \frac{A_0}{N_0} \times N_{\mathrm{d}} \times 100 \quad \% \tag{12}$$

2.4. Statistical method

All experimental results were analyzed using the SAS software (version 9.2, SAS Institute, Cary, NC, USA), and the significance level was set to 0.05 ($p = 0.05$). First, the fruit temperature, drop height, and initial drop direction of the fruit model were considered as potential independent variables. In the analysis process, the initial drop direction of the strawberry fruit was defined as a qualitative variable, which is classified and coded before analysis. The two initial directions, "along the transverse equatorial section" and "along the longitudinal equatorial section," were coded as "0" and "1", respectively, and the fruit temperature and drop height were designated as quantitative variables. The five parameters characterizing a strawberry drop-damage sensitivity, namely the maximum impact force of the fruit dropping onto a rigid surface, the maximum stress in the fruit, the fruit damage area, the fruit damage volume, and the percentage of damage volume were defined as dependent variables, and the covariance analysis method was used to investigate the factors influencing the drop-damage sensitivity of the strawberry fruit. The Fisher least significant difference (LSD) method in the multiple comparison test was used to determine whether there was a significant difference between the two initial drop directions. The common expression of the covariance analysis model is shown in Eq. (13) (Ruan, 2009).

$$P_i = \alpha_0 + \sum_{k=1}^{m_0} \alpha_{1k} C_{ik} + \sum_{j=1}^{n} \alpha_{2j} x_{ij} + \varepsilon_i \tag{13}$$

Subsequently, to investigate the relationship between strawberry fruit internal and surface damage, the damage volume and percentage of damage volume were used to express the fruit internal damage level regarded as dependent variables. The fruit damage area was used to describe the fruit surface damage level, considered the independent variable. According to the free drop FE simulation results of the strawberry fruit, the linear regression analysis method was carried out to establish the mathematical models between the damage volume of fruit and tissue and the fruit damage area, as well as between the percentage of damage volume of fruit and tissue and the fruit damage area.

3. Results and discussions

3.1. Validation of the finite element model

Fig. 3e shows the von Mises stress distribution of the cortex and pith tissues in the transverse equatorial section of a strawberry fruit after a free drop from a height of 411 mm ($v = 3\ \mathrm{m{\cdot}s^{-1}}$) to the rigid surface. In the fruit FE model, the elastic modulus, yield stress, Poisson's ratio, and density of the cortex tissue were 0.373 MPa, 0.061 MPa, 0.40, and 1.01 $\mathrm{g{\cdot}cm^{-1,}}$ respectively; the elastic modulus, yield stress, Poisson's ratio and density of the pith tissue were 0.448 MPa, 0.070 MPa, 0.40 and 1.01 $\mathrm{g{\cdot}cm^{-1}}$ respectively. During the collision process of the fruit model dropping onto the rigid surface, the maximum von Mises stress of the cortex and pith tissues were 0.190 MPa and 0.163 MPa, respectively. The gray region in the cortex and pith models indicated that the region's von Mises stress value was greater than its tissue yield stress, which stands for the damage region of the corresponding tissue. Clearly, most of the damaged regions of the cortex and pith model were located inside the fruit. If the fruit model is not sectioned, it is difficult to observe the fruit's internal mechanical damage status and degree.

Table 2 shows the simulation results of the strawberry fruit after a free drop from a height of 411 mm ($v = 3\ \mathrm{m{\cdot}s^{-1}}$) to the rigid surface when the cortex and pith model was inputted with the maximum, average, and minimum measured mechanical values, as well as the 5 repeated free drop experimental results at room temperature. Evidently, when the elastic modulus and yield stress of the strawberry cortex and pith tissue model are at their average values in the experimental measurements, the relative error between the simulation results and the experimental results is small, and the relative errors of the maximum impact force, maximum contact area between fruit and rigid surface, fruit damage area and percentage of damage volume of the strawberry fruit after the collision were − 1.76%, − 8.45%, − 2.99%, and 4.74%, respectively. Hence, the model has a high prediction accuracy and will be further used in the following research on strawberry drop-damage sensitivity analysis.

Table 2
Experimental and FE simulation results of the fruit free drop onto a rigid surface.

Mechanical Parameters	F_{max} (N)		Error (%)	A_c (mm^2)		Error (%)	A_d (mm^2)		Error (%)	P_{dvf} (%)		Error (%)
	Experiment	Simulation		Experiment	Simulation		Experiment	Simulation		Experiment	Simulation	
$E_c = E_{maxc}$, $E_p = E_{maxp}$ $\sigma_{yc} = \sigma_{maxyc}$, $\sigma_{yp} = \sigma_{maxyp}$	44.77 ± 9.44	43.61	2.60	525.59 ± 25.61	568.32	-8.13	174.88 ± 19.53	195.32	-11.69	8.22 ± 1.12	8.65	-5.23
$E_c = E_{avgc}$, $E_p = E_{avgp}$ $\sigma_{yc} = \sigma_{avgyc}$, $\sigma_{yp} = \sigma_{avgyp}$	44.77 ± 9.44	45.56	-1.76	525.59 ± 25.61	570.01	-8.45	174.88 ± 19.53	180.11	-2.99	8.22 ± 1.12	7.83	4.74
$E_c = E_{minc}$, $E_p = E_{minp}$ $\sigma_{yc} = \sigma_{minyc}$, $\sigma_{yp} = \sigma_{minyp}$	44.77 ± 9.44	47.83	-6.83	525.59 ± 25.61	575.86	-9.56	174.88 ± 19.53	167.33	4.32	8.22 ± 1.12	7.24	15.57

Note: the "error" is the percentage of the relative error between simulation and experiment result.

Fig. 4 shows the two drop-rebound simulation processes of the strawberry fruit FE model dropping from a height of 411 mm (v = 3 m·s^{-1}) onto the rigid surface. Fig. 4a shows the von Mises stress status of the strawberry fruit at 5 positions (21st, 25th, 1539th, 3975th, 3980th step) during two drop-rebound processes. The collision speed of the strawberry fruit decreased to 0 for the first time at the 21st step, and the impact force of the fruit model to the rigid surface reached its maximum value, with maximum contact stress appearing in the cortex and pith tissue model of 0.097 and 0.142 MPa, respectively (Fig. 4b and c). In the 25th step, the strawberry fruit model is in the elastic recovery stage during collision, where the elastic potential energy of the fruit is reduced, most of which is converted into kinetic energy for upward movement, and at the same time, the center of gravity of the fruit has moved upward from the lowest point, its velocity is greater than 0, and the direction is opposite to that in the compression phase. At the 1539th step, the strawberry fruit rebounded up to the highest point, h_2, the velocity decreased to 0, the fruit model had no contact with the rigid surface, and the internal stress values of the cortex and pith tissue models decreased (Fig. 4b and c). At the 3975th step, the collision speed of the strawberry fruit decreased to 0 for the second time, and the maximum contact stress inside the cortex and pith tissue models were 0.081 and 0.045 MPa, respectively (Fig. 4b and c). Here, the duration between the start of rebounding after the first drop and contact with the rigid surface before the second collision approximates 510 ms. At the 5382nd step, the strawberry fruit rebounded upward to the highest point, h_3, the collision speed decreased to 0, the fruit model had no contact with the rigid surface, and the maximum stress values of the cortex and pith tissue models were 0.081 and 0.033 MPa, respectively (Fig. 4b and c). Possibly owing to the effect of the shock wave, the strawberry fruit's posture on the second drop (3975th step) differed from that on the first drop (21st step), and the fruit surface morphological characteristics also differed between the compression stage

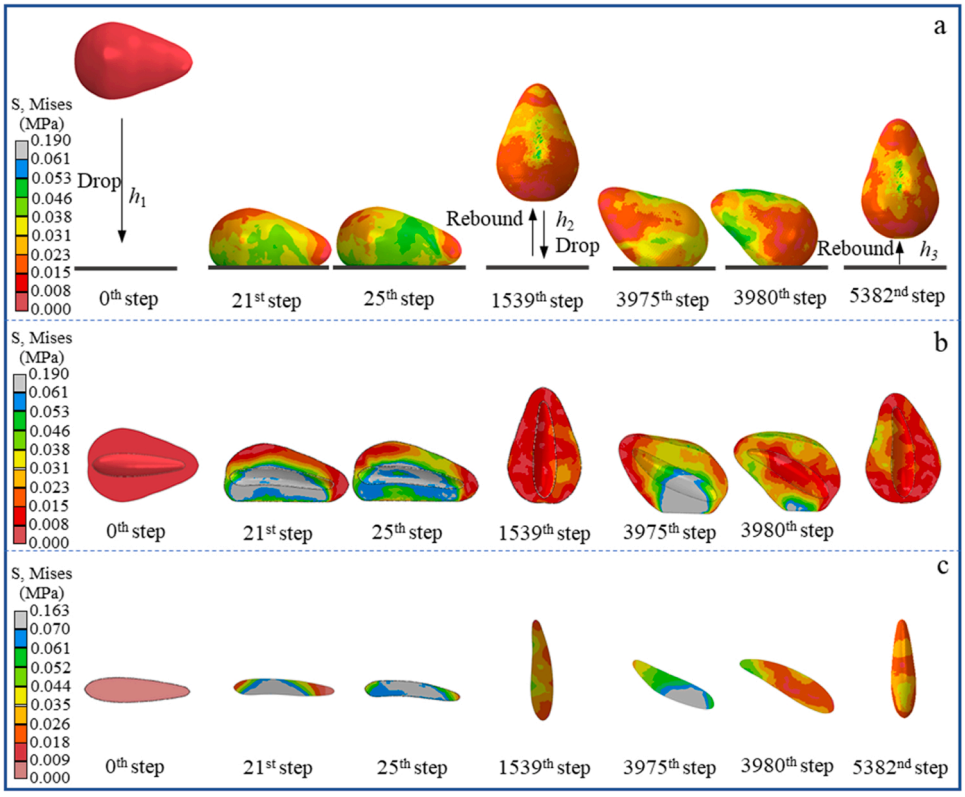

Fig. 4. Two drop-rebound processes of a fruit model in free drop simulation. (a) von Mises stress change of fruit in the drop – rebound – drop – rebound process, (b) von Mises stress change of the cortex tissue in fruit equatorial section, (c) von Mises stress change of the pith tissue in fruit equatorial section.

(3975th step) and the recovery stage (3980th step) during the second drop.

3.2. Sensitivity of the dynamic finite element model

3.2.1. Sensitivity of the FE model to fruit mechanical properties

The collision process of the strawberry fruit model dropping onto the rigid ground can be divided into two stages: compression and recovery (Li et al., 2017b). The compression stage is the period between when the fruit first makes contact with the rigid surface and when the fruit experiences maximum impact force (maximum deformation). During this period, the impact velocity of the fruit reduced from 3 m·s^{-1} to 0. The recovery stage is the process of recovering the deformation caused by the fruit colliding with the rigid surface, during which the impact velocity of the fruit rose from 0 to the maximum value (Fig. 5a). Fig. 5b shows the *F-t* curve of impact force change with contact time during the fruit free drop onto the rigid surface when the elastic modulus and yield stress of the cortex tissue and pith tissue are at average values (E_{yc} = 0.373 MPa, E_{yp} = 0.448 MPa, σ_{yc} = 0.061 MPa, σ_{yp} = 0.070 MPa), 20% higher value (E_{yc} = 0.448 MPa, E_{yp} = 0.538 MPa, σ_{yc} = 0.073 MPa, σ_{yp} = 0.084 MPa), and 20% lower value (E_{yc} = 0.298 MPa, E_{yp} = 0.358 MPa, σ_{yc} = 0.049 MPa, σ_{yp} = 0.056 MPa). The impact force of the strawberry fruit model on the rigid surface increases with contact time in the compression stage; in the recovery stage, the impact force of the

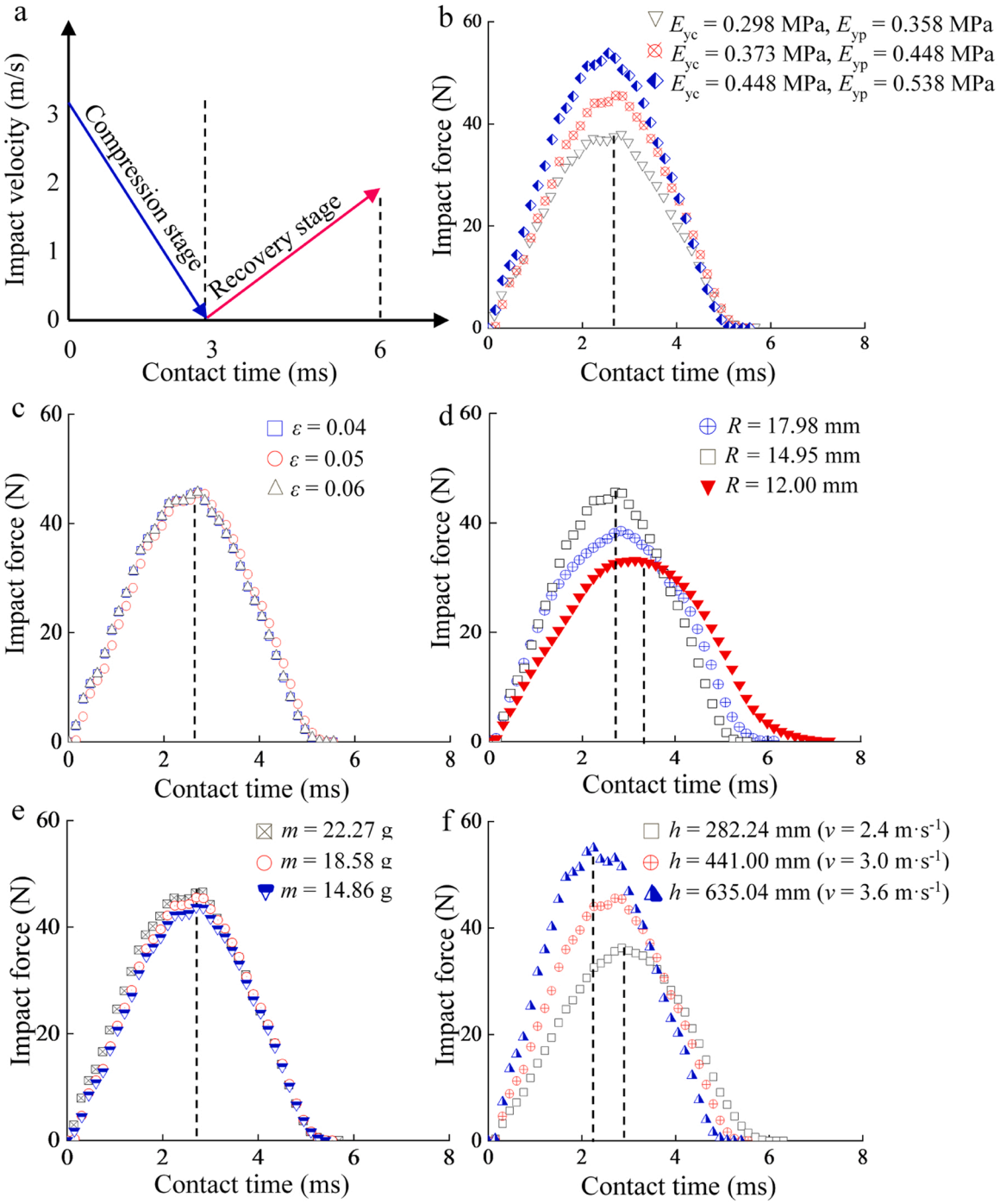

Fig. 5. Sensitivity analysis of the dynamic finite element model. (a) Two stages of the collision process in a fruit free drop test, (b) ~ (f) Sensitivity of the FE model to tissue elastic modulus, tissue plastic strain, fruit curvature radius, fruit mass, and fruit drop height, respectively.

strawberry fruit model on the rigid surface decreases with contact time. However, the impact force of the strawberry fruit model free drop onto the rigid surface has a nonlinear relationship with contact time change which slowly increases to the maximum value in the late compression stage and slowly decreases to 0 in the late recovery stage.

The maximum impact force of the strawberry fruit model free drop onto the rigid surface increases as the elastic modulus and yield stress of the cortex tissue and pith tissue increase, while the impact contact time between the fruit and the rigid surface remains constant at roughly 5.60 ms. When the elastic modulus and yield stress of the cortex tissue and pith tissue were $E_{yc} = 0.448$ MPa, $E_{yp} = 0.538$ MPa, $\sigma_{yc} = 0.073$ MPa, $\sigma_{yp} = 0.084$ MPa, respectively, the maximum impact force of the strawberry fruit model free drop onto the rigid surface was 53.86 N, 1.42 times higher than when $E_{yc} = 0.298$ MPa, $E_{yp} = 0.358$ MPa, $\sigma_{yc} = 0.049$ MPa, $\sigma_{yp} = 0.056$ MPa, $\sigma_{yp} = 0.056$ MPa. However, the time from the collision between the fruit and the rigid surface to the peak impact force is all about 2.70 ms under the two mechanical parameter settings. That is, the contact time in the compression stage of the strawberry on the rigid surface collision process is about 2.70 ms, and the contact time in the recovery stage of the strawberry fruit on the rigid ground collision process is about 2.90 ms. Therefore, the contact period of the strawberry fruit with the rigid surface during the recovery stage is greater than that during the compression stage. Fig. 5c shows the *F-t* curve of the change in impact force of the strawberry fruit model free drop onto the rigid surface with contact time when the plastic strains of the cortex tissue and the pith tissues are 0.04, 0.05, and 0.06, respectively. The results show that as the plastic strain of the cortex and pith tissues increased, there was almost no significant difference in the maximum impact force of the strawberry fruit model free drop onto the rigid surface, which was approximately 45.50 N; and the impact contact time between the fruit and the rigid surface was approximately 5.60 ms, which did not change significantly.

In summary, the impact force was more sensitive to the mechanical parameters of the fruit material during the elastic stage but insensitive to the plastic strain after the fruit was damaged. However, the contact time of the strawberry fruit free drop finite element model on the rigid surface was not sensitive to the fruit material's elastic-plastic mechanical parameters. According to the existing literature, the maximum impact force when kiwifruit, pear, and apple fruit free drop onto a rigid surface varies with the elastic modulus, and the contact times were 4.50 ms, 5.50 ms, and 4.80 ms, respectively (Celik, 2017; Du et al., 2019; Stropek and Gołacki, 2013). The elastic modulus of the fruit reflects its firmness characteristics. Fruit firmness decreases with increasing maturity (Du et al., 2019), and the firmer the fruit free drop onto the rigid surface, the greater the impact force. There have been few investigations on the influence of varying plastic strains on the maximum impact force of the fruit free drop onto the rigid surface as well as the contact time between the fruit and the rigid surface. Plastic strain is the residual strain that remains after the external force acting on the material has been removed. This might be because fruit and vegetable biomass materials are delicate when they break, and it is challenging to measure plastic strain with current technologies. The plastic strain values for the strawberry cortex and pith tissues described in this study are estimations and are offered solely for reference purposes.

3.2.2. Sensitivity of the FE model to fruit properties

Fig. 5d shows that the *F-t* curve of the change in impact force of the strawberry fruit model free drop onto the rigid surface with contact time at the initial contact position on the transverse equatorial section of the fruit with a radius of curvature $R = 14.95$ mm, increased by 20% ($R = 17.98$ mm) and decreased by 20% ($R = 12.00$ mm). As the curvature radius of the initial location of the fruit model free drop onto the rigid surface increases, so does the collision contact time between the fruit model and the rigid surface. When the curvature radius of the initial contact point of the fruit was $R = 12.00$ mm, the collision contact time between the fruit model and the rigid surface was 7.35 ms, which is 1.32 times higher than at the curvature radius of the initial contact point $R = 17.98$ mm. The curvature radius of the fruit model's initial contact point has an obvious impact on the maximum impact force of the strawberry fruit model free-dropping on the rigid surface. When the radius of curvature of the initial contact point of the fruit model was $R = 14.95$ mm, the maximum impact force between the fruit model and the rigid surface was 45.57 N, which is 1.38 times and 1.19 times higher than at $R = 12.00$ mm and $R = 17.98$ mm, respectively.

Fig. 5e shows the *F-t* curve of the change in impact force of the strawberry fruit model free drop onto the rigid surface with contact time when the free-drop fruit mass is average ($m = 18.58$ g), increased by 20% ($m = 22.27$ g), and decreased by 20% ($m = 14.86$ g). With an increase in the strawberry fruit mass, the maximum impact force of the strawberry fruit model free drop on the rigid surface, and the collision contact time between the fruit and the rigid surface increased slightly. When the fruit model mass was 22.27 g, the maximum impact force of the strawberry fruit model free drop on the rigid surface was 46.57 N, and the collision contact time between the fruit model and the rigid surface was 5.69 ms, which is 1.06 times and 1.05 times higher than when $m = 14.86$, respectively.

In summary, the impact force of the strawberry fruit model dropped onto the rigid surface and the contact time between the fruit and the rigid surface are more sensitive to the fruit surface morphology but less sensitive to the mass of the fruit (Fig. 5). The reason is that the surface morphology of strawberry fruit varies greatly, while the fluctuation range of strawberry fruit mass is relatively narrow. An et al. (2020) found that the mechanical damage near the strawberry fruit stalk (large radius of curvature) was significantly greater than that near the fruit tip (small radius of curvature) near the stem flower point when compressed from flat plates on both sides of the strawberry along the stem and flower axis. It demonstrates that the tissue near the strawberry fruit stem is less resistant to external force than the tissue at the strawberry fruit tip due to the spatial distribution characteristics and hierarchical structural mechanics of different tissues inside the fruit. A similar result was reported in Celik (2017) for pear, in that the collision contact time is different when a fruit drops from two directions onto the ground. Almost no previous literature on fruit free drop and collision showed the influence of fruit mass on the impact force and contact time in the collision process between fruit and object. According to the law of conservation of momentum, the fruit model free drop with a large mass will have a larger impulse to the rigid surface under the same impact velocity. When the contact time between the fruit and the rigid surface is nearly equal, the fruit model's maximum impact force on the rigid surface is greater (Li et al., 2017a).

3.2.3. Sensitivity of the FE model to drop height

Fig. 5f shows that the *F-t* curve of the impact force of the strawberry fruit model free drop onto the rigid surface changed with contact time when the strawberry fruit model was dropped from heights of 635, 411, and 282 mm, with corresponding initial collision velocities of 3.6, 3.0, and 2.4 $m \cdot s^{-1}$, respectively. The maximum impact force of the fruit model on the rigid surface decreases as the free drop height of the fruit model decreases, and the collision contact time between the fruit model and the rigid surface increases. When the fruit drop height was 635 mm, the maximum impact force between the fruit model and the rigid surface was 54.98 N, and the collision contact time was 6.31 ms, which is 1.54 times and 0.85 times more than when the height was 282 mm, respectively. Similar results were found in these studies: Stropek and Gołacki (2013) for apples, Yousefi et al. (2016) for pears, in that there was a positive correlation between the drop height (or initial collision velocity) and maximum impact force of fruit. The reason may be related to the mechanical failure properties of fresh fruit biomaterial. According to the law of conservation of momentum, the higher the drop height of the same mass fruit, the greater the impulse to the rigid surface, the impact damage of the fruit material has hysteresis, and the faster the rebound

velocity.

3.3. Prediction of the drop-damage sensitivity of strawberry fruit

3.3.1. Factors affecting the drop damage sensitivity of strawberry fruit

Five covariance analysis models are shown in Table 3. All the coefficients of determination R^2 were larger than 0.90, indicating that during the strawberry fruit free drop, the corresponding covariance analysis model could predict more than 90% of the independent variable changes. Overall, the three independent variables (fruit temperature, drop height, and initial drop direction) had a significant effect on the five dependent variables in the obtained covariance analysis models ($p < 0.05$). This observation illustrated that the initial drop direction, fruit temperature, and drop height were the sensitive indicators affecting the drop damage characteristics of strawberry fruit.

In the free drop simulation of the strawberry fruit, the maximum impact force of the strawberry fruit dropped onto the rigid surface, and the maximum stress in the fruit gradually decreased as the fruit temperature increased. When the fruit temperature increased by 1 °C, the maximum impact force of the strawberry fruit and the maximum stress decreased by 0.32 N and 0.0019 MPa, respectively. The maximum impact force of the strawberry fruit dropping onto the rigid surface and the maximum stress in the fruit gradually increased as the drop height of the fruit increased. When the drop height increased by 1 mm, the maximum impact force of the fruit and the maximum stress increased by 0.08 N and 0.0002 MPa, respectively. The maximum impact force and stress of the strawberry fruit dropping onto the rigid surface differ significantly depending on the initial drop direction. Furthermore, the maximum impact force and stress of the fruit dropping along the longitudinal equatorial section onto the rigid surface were reduced by 4.01 N and 0.0177 MPa, respectively, compared to those along the transverse equatorial section. In the relatively low temperature range of 1–7 ℃, the drop damage indexes of strawberry fruit (*e.g.*, fruit damage area, fruit damage volume, and percentage of damage volume) had no significant difference ($p > 0.05$) with the increase in temperature. However, when the fruit temperature was between 14 °C and 35 °C, the drop damage indexes of strawberry fruit increased significantly with the increase in fruit temperature ($p < 0.05$). As a result, a two-stage function was obtained to represent the covariance analysis model for predicting the drop-damage sensitivity of strawberry fruit using damage area, damage volume, and percentage of damage volume as dependent variables. In the temperature range of 1–7 ℃, when the drop height increased by 1 mm, the damage area, damage volume, and percentage of damage volume of strawberry fruit increased by 0.45 mm^2, 4.03 mm^3, and 0.02%, respectively. When the fruit drops onto the rigid surface along the longitudinal equatorial section, the damage area, damage volume and percentage of damage volume of the fruit are reduced by 30.10 mm^2, 165.06 mm^3 and 0.89%, respectively, than those along the transverse equatorial section. When the fruit temperature was between 14 °C and 35 °C, the damaged area, damaged volume, and percentage of damage volume of strawberry fruit increased by 0.82 mm^2, 11.70 mm^3, and 0.06% for every 1 °C increase in fruit temperature. Additionally, the damage area, damage volume, and damage percentage increased by 0.43 mm^2, 3.88 mm^3, and 0.02%, respectively, for every 1 mm increase in drop height. Also, when the fruit dropped onto the rigid surface along the longitudinal equatorial section, the damage area, damage volume, and percentage of damage volume were reduced by 31.28 mm^2, 188.08 mm^3, and 1.01%, respectively, compared to dropping along the transverse equatorial section.

In summary, the factors influencing the strawberry fruit drop damage include the fruit characteristics (*e.g.*, temperature, size, surface shape, and ripeness) and external factors, such as drop height and initial drop direction. It can be seen from Table 1 that when the fruit temperature rises, the elastic modulus of the fruit tissue gradually decreases, making the drop damage characteristics of the strawberry fruit highly sensitive to temperature. In addition, the maximum impact force and the maximum von Mises stress of the strawberry fruit appear simultaneously during a fruit drop collision. There is a similar changing trend in the impact force and internal stress of the fruit dropping onto the rigid surface with increasing collision contact time. Previous literature, such as research by Du et al. (2019) and Celik (2017) on free drop damage of kiwifruit and pear, found that the drop damage of fruit is directly connected to drop direction, height, and maturity, which is similar to the research result in this study, but they did not consider the fruit temperature effects.

In a low temperature range (1 ~ 7 °C), the yield stress of the strawberry fruit is large, the ability to resist plastic deformation is strong, and the fruit is not easily damaged after free drop. Hence, the fruit damage area, damage volume, and percentage of damage volume for whole fruit did not change significantly with temperature change. The impact damage of a fruit free drop is caused mostly by the large instantaneous impact force to the impact surface. When the fruit temperature increases, the elastic modulus of the fruit drops significantly, as do the hardness of the fruit and the toughness of the cortex; this reduces the capacity of strawberry pulp to withstand transient shocks (Ferreira et al., 2009). Therefore, when the fruit temperature ranges from 14° to 35°C, the damage area, damage volume, and percentage of damage volume increase as the temperature rises. Similar results were reported in Banks and Joseph (1991), where the impact damage of bananas increased with temperature increase, and the impact energy (104 mJ) at 30 °C was 1.41 times higher than that at 19 °C.

The initial collision speed of the fruit dropping onto the rigid surface depended on the drop height. The higher the drop height, the greater the initial collision speed between the fruit free drop and the rigid surface, the greater the impact force of the fruit to the rigid surface, and the greater the initial kinetic energy of the fruit in the collision process with the rigid surface, and consequently, the greater the impact energy of the fruit. According to several studies, there is a linear correlation between the bruise volume and the impact energy of fruit (Van Linden et al., 2006), so the damage area, damage volume, and percentage of damage volume for whole fruit free drop will increase as drop height increases. The effect of drop direction on fruit damage may be induced by a difference in curvature radius at the initial collision point of a fruit free drop. When the fruit impacts the rigid surface along the longitudinal equatorial plane of the fruit, the curvature radius of the fruit at the collision contact point is greater than the curvature radius along the

Table 3
Five covariance analysis models with the maximum impact force, maximum stress, fruit damage area, fruit damage volume and percentage of damage volume as the dependent variable, respectively.

No.	Covariance analysis model	R^2
1	$F_{max} = -0.32\,T + 0.08\,h + 4.01\,d + 14.57$	0.94
2	$\sigma_{max} = -0.0019\,T + 0.0002\,h + 0.0177\,d + 0.0822$	0.90
3	$A_d = \begin{cases} 0.46\,h + 30.10\,d - 43.78 & (1 \le T \le 7) \\ 0.82\,T + 0.43\,h + 31.28\,d - 62.11 & (14 \le T \le 35) \end{cases}$	0.94
4	$V_{df} = \begin{cases} 4.03\,h + 165.06d - 381.23 & (1 \le T \le 7) \\ 11.70\,T + 3.88h + 188.08\,d - 660.76 & (14 \le T \le 35) \end{cases}$	0.94
5	$P_{dvf} = \begin{cases} (0.02h + 0.89\,d - 2.05) \times 100\ \% & (1 \le T \le 7) \\ (0.06\,T + 0.02\,h + 1.01\,d - 3.56) \times 100\ \% & (14 \le T \le 35) \end{cases}$	0.94

transverse equatorial plane of the fruit, so the fruit drop direction has a significant effect on the damage area, damage volume, and percentage of damage volume of the fruit. Similar findings were reported in studies on kiwifruit and pear. The damage volume of kiwifruit fruit free drop from a height of 0.50 m along the transverse equatorial section was 4144.2 mm^3, which was 2.21 times higher than that of the free drop from a height of 0.25 m, which was 1.63 times higher than that of the drop along the longitudinal equatorial section (Du et al., 2019). The damage percentage (8.15%) of pear fruit drop from a height of 0.50 m along the transverse equator section is 2.09 times higher than that of the drop from a height of 0.25 m. Also, the damage volume of pear fruit drop along the transverse equatorial section from a height of 0.25 m is 8379 mm^3, which is 1.08 times higher than the drop along the longitudinal equatorial section (Celik, 2017).

3.3.2. Prediction of the relationship between internal and surface damage of strawberry fruit

The correlation between fruit damage volume or percentage of damage volume and damage area of a dropped strawberry reflects the relationship between internal and external damage of the dropped fruit. There were two free drop directions: fruit dropped along the transverse equatorial section (Fig. 6a and b) and the longitudinal equatorial section (Fig. 6c and d) in the simulation. Regardless of the direction in which the fruit was dropped, the fruit damage volume and percentage of damage volume (standing for the internal damage) demonstrated a positive linear correlation with the fruit damage area (standing for the surface damage). The damage volume (Fig. 6a and c) and percentage of damage volume (Fig. 6b and d) of the cortex tissue gradually differed from those of the pith tissue as the damaged area of the fruit surface increased. The reason can be attributed to the fact that the cortex tissue is located on the fruit's exterior, and it directly contacts and deforms locally with the rigid surface during the collision process of the fruit dropping onto the rigid surface. Besides, the ability of the cortex to resist external forces becomes relatively poor because the elastic modulus of the cortex tissue is significantly lower than that of the pith tissue. When the slopes of the linear regression equations for the fruit damage volume *vs* damage area curves in Fig. 6a and c were compared, it was found that the damage velocity of the strawberry fruit dropping onto the rigid surface along the longitudinal equatorial section was greater than that dropping along the transverse equatorial section. There is no information about the relationship between internal and external strawberry damage in the literature, so no comparisons are possible.

4. Conclusion

In this study, a strawberry drop finite element model was developed. Results showed that the fruit finite element model with average tissue mechanical data could replicate four key collision mechanical parameters (maximum impact force and contact area, drop damage area, percentage of damage volume). The covariance analysis revealed that the drop direction was the most important independent variable affecting the occurrence of the fruit drop damage, followed by the fruit temperature and drop height. The fruit damage degree did not change significantly with temperature change in the low temperature range (1 ~ 7 °C)

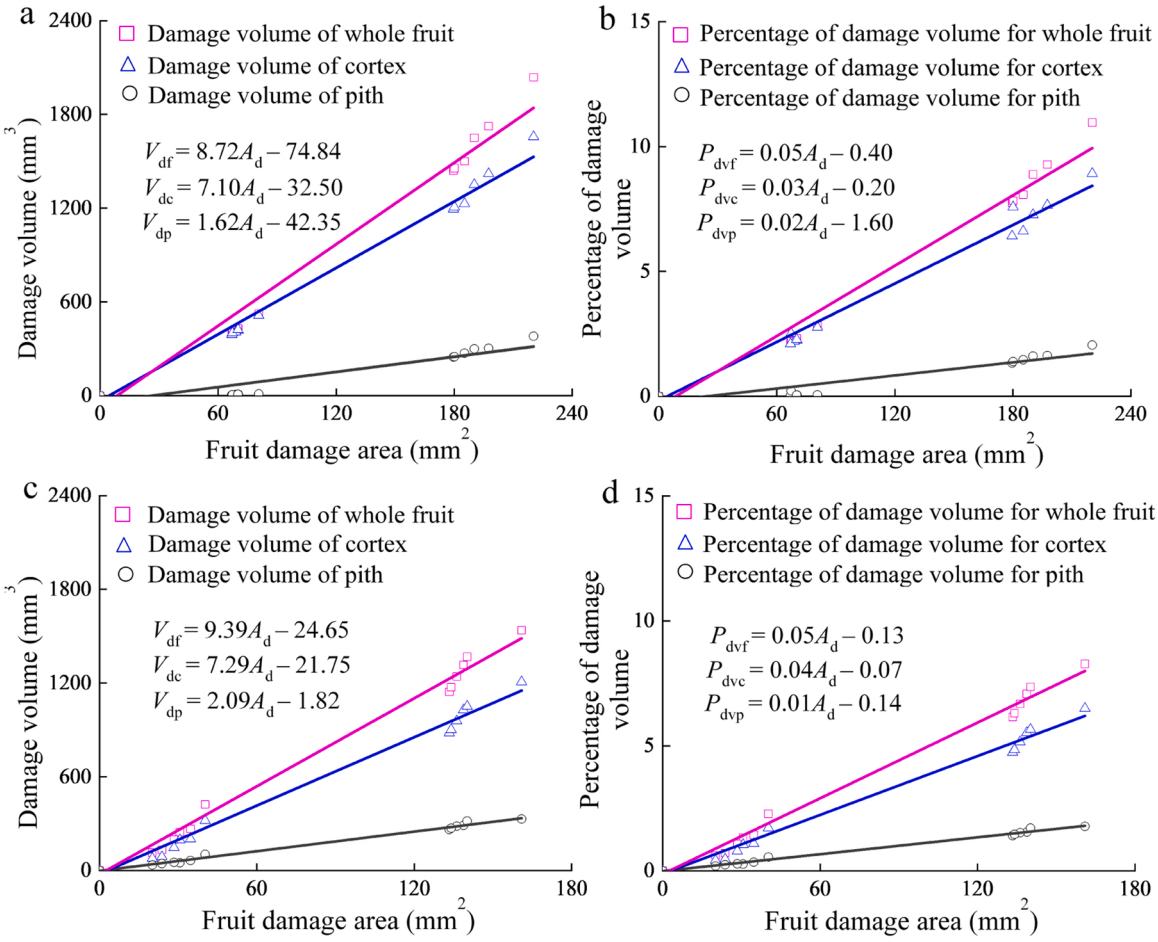

Fig. 6. Correlation between damage volume and damage area of a dropped strawberry. (a) damage volume *vs* damage area of fruit dropping along the transverse equatorial section, (b) percentage of damage volume *vs* damage area of fruit dropping along the transverse equatorial section, (c) damage volume *vs* damage area of fruit dropping along the longitudinal equatorial section, (d) percentage of damage volume *vs* damage area of fruit dropping along the longitudinal equatorial section.

but increased as the temperature rises in the temperature ranging from 14° to 35°C. Finally, when the internal and surface damage of fruit were quantified using the fruit damage volume and damage area, respectively, it was observed that there was a strong linear relationship between internal and surface damage of dropped strawberry fruit. The obtained mathematical models can be used to predict the internal damage degree of fruit based on the surface damage area in fruit grading factories' online non-destructive detection system. The dynamic collision occurs in a very short contact time, so this work reflected that the FE prediction is a powerful complementary method to actual experiments for objectively assessing some collision mechanical damage characteristics.

CRediT authorship contribution statement

Xue An: Conceptualization, Investigation, Resources, Data curation, Software, Validation, Writing – original draft. **Huijie Liu:** Writing – review & editing. **Tobi Fadiji:** Writing – review & editing, Supervision. **Zhiguo Li:** Writing – review & editing, Supervision, Funding acquisition, Project administration. **Darko Dimitrovski:** Supervision.

Declaration of Competing Interest

The authors declare that they have no known competing financial interests or personal relationships that could have appeared to influence the work reported in this paper.

Acknowledgments

This work was supported by a European Marie Curie International Incoming Fellowship (326847 and 912847), a Chinese Universities Scientific Fund (2452018313), and a Chinese-Macedonian Scientific and Technological Cooperation project (2019–6-9).

References

Aliasgarian, S., Ghassemzadeh, H.R., Moghaddam, M., Ghaffari, H., 2015. Mechanical damage of strawberry during harvest and postharvest operations. Acta Technol. Agricult. 18, 1–5. https://doi.org/10.1515/ata-2015-0001.

An, X., Li, Z., Zude-Sasse, M., Tchuenbou-Magaia, F., Yang, Y., 2020. Characterization of textural failure mechanics of strawberry fruit. J. Food Eng. 282, 110016 https://doi.org/10.1016/j.jfoodeng.2020.110016.

Banks, N.H., Joseph, M., 1991. Factors affecting resistance of banana fruit to compression and impact bruising. Sci. Food Agricult. 56 (3), 315–323. https://doi.org/10.1002/jsfa.2740560307.

Belytschko, T., Liu, W.K., Moran, B., 2000. Nonlinear Finite Elements for Continua and Structures. Wiley,, England, pp. 278–286.

Bovi, G.G., Caleb, O.J., Ilte, K., Rauh, C., Mahajan, P.V., 2018. Impact of modified atmosphere and humidity packaging on the quality, off-odour development and volatiles of '*Elsanta*' strawberries. Food Packag. Shelf Life 16, 204–210. https://doi.org/10.1016/j.fpsl.2018.04.002.

Celik, H.K., 2017. Determination of bruise susceptibility of pears (*Ankara* variety) to impact load by means of FEM-based explicit dynamics simulation. Postharvest Biol. Technol. 128, 83–97. https://doi.org/10.1016/j.postharvbio.2017.01.015.

Celik, H.K., Rennie, A.E.W., Akinci, I., 2011. Deformation behaviour simulation of an apple under drop case by finite element method. J. Food Eng. 104, 293–298. https://doi.org/10.1016/j.jfoodeng.2010.12.020.

Chaiwong, S., Bishop, C.F., 2015. Effect of vibration damage on the storage quality of '*Elsanta*' strawberry. Aus. J. Crop Sci. 9, 859–864. https://doi.org/10.1016/0197-4580(90)90066-9.

Chang, Y.C., Lin, T.C., 2020. Temperature effects on fruit development and quality performance of nagami kumquat (*Fortunella margarita* [Lour.] Swingle). Horticult. J. 89, 351–358. https://doi.org/10.2503/hortj.UTD-120.

Chockchaisawasdee, S., Golding, J.B., Vuong, Q.V., Papoutsis, K., Stathopoulos, C.E., 2016. Sweet cherry: composition, postharvest preservation, processing and trends for its future use. Trends Food Sci. Technol. 55, 72–83. https://doi.org/10.1016/j.tifs.2016.07.002.

Deng, W., Wu, J., Da, Y., Ma, Z., 2020. Effect of temperature treatment on fruit quality and immunoregulation of Satsuma (*Citrus unshiu* Marc.) during storage. Food Sci. Nutr. 8, 5443–5451. https://doi.org/10.1002/fsn3.1771.

Dintwa, E., Van Zeebroeck, M., Ramon, H., Tijskens, E., 2008. Finite element analysis of the dynamic collision of apple fruit. Postharvest Biol. Technol. 49, 260–276. https://doi.org/10.1016/j.postharvbio.2008.01.012.

Du, D., Wang, B., Wang, J., Yao, F., Hong, X., 2019. Prediction of bruise susceptibility of harvested kiwifruit (*Actinidia chinensis*) using finite element method. Postharvest Biol. Technol. 152, 36–44. https://doi.org/10.1016/j.postharvbio.2019.02.013.

Duarte-Molina, F., Gómez, P.L., Castro, M.A., Alzamora, S.M., 2016. Storage quality of strawberry fruit treated by pulsed light: Fungal decay, water loss and mechanical properties. Innov. Food Sci. Emerg. Technol. 34, 267–274. https://doi.org/10.1016/j.ifset.2016.01.019.

Dzidek, B.M., Adams, M.J., Andrews, J.W., Zhang, Z., Johnson, S.A., 2017. Contact mechanics of the human finger pad under compressive loads. J. R. Soc. Interface 14, 13. https://doi.org/10.1098/rsif.2016.0935.

FAOSTAT (2020). ⟨http://www.fao.org/faostat/zh/#data/QC⟩.

Ferreira, M.D., Sargent, S.A., Brecht, J.K., Chandler, C.K., 2009. Strawberry bruising sensitivity depends on the type of force applied, cooling method, and pulp temperature. Hortscience 44, 131–144. https://doi.org/10.21273/HORTSCI.44.7.1953.

Guo, X., Luo, T., Han, D., Wu, Z., 2019. Analysis of metabolomics associated with quality differences between room-temperature and low-temperature-stored litchi pulps. Food Sci. Nutr. 7, 3560–3569. https://doi.org/10.1002/fsn3.1208.

Han, X., An, X., Fadiji, T., Li, Z., Khojastehpour, M., 2022. Textural thermo-mechanical properties of sweet cherry for postharvest damage analysis. J. Texture Stud. 1–12. https://doi.org/10.1111/jtxs.12661.

Hikawa-Endo, M., 2020. Improvement in the shelf-life of Japanese strawberry fruits by breeding and postharvest techniques. Horticult. J. 89, 115–123. https://doi.org/10.2503/hortj.UTD-R008.

Hussein, Z., Fawole, O.A., Opara, U.L., 2020. Harvest and postharvest factors affecting bruise damage of fresh fruits. Horticult. Plant J. 6, 1–13. https://doi.org/10.1016/j.hpj.2019.07.006.

Jiang, Y., Duan, X., Qu, H., Zheng, S., 2016. Browning: enzymatic browning. Encyclopedia Food Health 12, 508–514. https://doi.org/10.1016/B978-0-12-384947-2.00090-8.

Kelly, K., Madden, R., Emond, J.P., Do Nascimento Nunes, M.C., 2019. A novel approach to determine the impact level of each step along the supply chain on strawberry quality. Postharvest Biol. Technol. 147, 78–88. https://doi.org/10.1016/j.postharvbio.2018.09.012.

Kurpaska, S., Sobol, Z., Pedryc, N., Hebda, T., Nawara, P., 2020. Analysis of the pneumatic system parameters of the suction cup integrated with the head for harvesting strawberry fruit. Sensors 20, 4389. https://doi.org/10.3390/s20164389.

Li, D., Li, Z., Tchuenbou-Magaia, F., 2021. An extended finite element model for fracture mechanical response of tomato fruit. Postharvest Biol. Technol. 174, 111468 https://doi.org/10.1016/j.postharvbio.2021.111468.

Li, Z., Andrews, J., Wang, Y., 2017a. Mathematical modelling of mechanical damage to tomato fruits. Postharvest Biol. Technol. 126, 50–56. https://doi.org/10.1016/j.postharvbio.2016.12.001.

Li, Z., Miao, F., Andrews, J., 2017b. Mechanical models of compression and impact on fresh fruits. Comprehensive Rev. Food Sci. Food Saf. 16, 1296–1312. https://doi.org/10.1111/1541-4337.12296.

Lin, J., Holmes, M., Vinson, R., Ge, C., Pogoda, F.C., Mahon, L., Gentry, R., Seibel, G.E., Chen, X., Tao, Y., 2017. Design and testing of an automated high-throughput computer vision guided waterjet knife strawberry calyx removal machine. J. Food Eng. 211, 30–38. https://doi.org/10.1016/j.jfoodeng.2017.05.002.

López-Serrano, M., Ros Barceló, A., 2001. Histochemical localization and developmental expression of peroxidase and polyphenol oxidase in strawberries. J. Am. Soc. Horticult. Sci. 126, 27–32. https://doi.org/10.21273/JASHS.126.1.27.

Mahiuddin, M., Godhani, D., Feng, L., Liu, F., Langrish, T., Karim, M.A., 2020. Application of caputo fractional rheological model to determine the viscoelastic and mechanical properties of fruit and vegetables. Postharvest Biol. Technol. 163, 111147 https://doi.org/10.1016/j.postharvbio.2020.111147.

Matsumoto, H., Ikoma, Y., 2012. Effect of different postharvest temperatures on the accumulation of sugars, organic acids, and amino acids in the juice sacs of satsuma mandarin (*Citrus unshiu* Marc.) fruit. J. Agricult. Food Chem. 60, 9900–9909. https://doi.org/10.1021/jf303532s.

Ruan, J., 2009. From entry to proficient in SAS statistical analysis. Posts & Telecom Press,, China.

Sadrnia, H., Rajabipour, A., Jafari, A., Javadi, A., Mostofi, Y., Kafashan, J., Dintwa, E., De Baerdemaeker, J., 2008. Internal bruising prediction in watermelon compression using nonlinear models. J. Food Eng. 86, 272–280. https://doi.org/10.1016/j.jfoodeng.2007.10.007.

Stropek, Z., Gołacki, K., 2013. The effect of drop height on bruising of selected apple varieties. Postharvest Biol. Technol. 85, 167–172. https://doi.org/10.1016/j.postharvbio.2013.06.002.

Surdilovic, J., Praeger, U., Herold, B., Truppel, I., Geyer, M., 2018. Impact characterization of agricultural products by fall trajectory simulation and measurement. Comput. Electron. Agricult. 151, 460–468. https://doi.org/10.1016/j.compag.2018.06.009.

Van Linden, V., De Ketelaere, B., Desmet, M., De Baerdemaeker, J., 2006. Determination of bruise susceptibility of tomato fruit by means of an instrumented pendulum. Postharvest Biol. Technol. 40, 7–14. https://doi.org/10.1016/j.postharvbio.2005.12.008.

Xanthopoulos, G., Koronaki, E.D., Boudouvis, A.G., 2012. Mass transport analysis in perforation-mediated modified atmosphere packaging of strawberries. J. Food Eng. 111, 326–335. https://doi.org/10.1016/j.jfoodeng.2012.02.016.

Xia, M., Zhao, X., Wei, X., Guan, W., Wei, X., Xu, C., Mao, L., 2020. Impact of packaging materials on bruise damage in kiwifruit during free drop test. Acta Physiol. Plantarum 42, 119. https://doi.org/10.1007/s11738-020-03081-5.

Yousefi, S., Farsi, H., Kheiralipour, K., 2016. Drop test of pear fruit: experimental measurement and finite element modelling. Biosyst. Eng. 147, 17–25. https://doi.org/10.1016/j.biosystemseng.2016.03.004.

Zhao, X., Xia, M., Wei, X., Xu, C., Luo, Z., Mao, L., 2019. Consolidated cold and modified atmosphere package system for fresh strawberry supply chains. LWT 109, 207–215. https://doi.org/10.1016/j.lwt.2019.04.032.

Zulkifli, N., Hashim, N., Harith, H.H., Mohamad Shukery, M.F., 2020. Finite element modelling for fruit stress analysis - A review. Trends Food Sci. Technol. 97, 29–37. https://doi.org/10.1016/j.tifs.2019.12.029.